Diagnosis of Cloud Mass and Heat Fluxes from Radar and Synoptic Data[1]

ROBERT A. HOUZE, JR., CHEE-PONG CHENG, COLLEEN A. LEARY[2] AND JOHN F. GAMACHE

Department of Atmospheric Sciences, University of Washington, Seattle 98195

(Manuscript received 31 July 1979, in final form 5 November 1979)

ABSTRACT

A set of equations for diagnosing the properties of precipitating clouds over a tropical ocean is developed by postulating a population of model clouds in which the vertical motions consist of convective updrafts and downdrafts in cumulus-scale cells and mesoscale updrafts and downdrafts associated with anvil clouds. The properties of a population of precipitating clouds can be diagnosed with these equations by constraining the model clouds to explain either an observed large-scale heat budget (the synoptic approach) or an observed spectrum of precipitation (the radar approach). The results of either approach are dependent on certain parameters of the model clouds, which must be assumed. These parameters are identified, and, in this paper, they are held constant in a controlled experiment comparing the results of the radar and synoptic approaches obtained for the same cloud population (the average population in Phase III of GATE). This experiment shows that similar results can be obtained by either approach, giving confidence in both sets of data, the methods used to analyze them and the diagnostic equations themselves. In this experiment, however, the model parameters were adjusted to suppress the diagnosis of the mesoscale motions associated with precipitating anvil clouds. In other papers, the model parameters will be varied to test the model dependency of the diagnostic calculations, especially with regard to the inclusion of mesoscale motions.

1. Introduction

One of the main objectives of the Global Atmospheric Research Programme's Atlantic Tropical Experiment (GATE) was a better understanding of the relationship of tropical convection to large-scale flow patterns. It is hoped that such an understanding, obtained through the analysis of observations obtained in GATE of both the convection and its large-scale environment, will lead to realistic methods of parameterizing the subgrid-scale convection in large-scale numerical models.

Toward this end, detailed studies of several of the convective systems in GATE have been undertaken (Zipser, 1977; Houze, 1977; Zipser and Gautier, 1978; Warner *et al.*, 1980; Leary and Houze, 1979a,b). These studies clearly indicate that the view of convection adopted in even the most elaborate convective parameterization schemes (e.g., Arakawa and Schubert, 1974) is considerably oversimplified. These schemes usually assume that the convection consists of a population of simple cumulus-scale updraft cylinders extending to various heights. The observational studies noted above, however, show that the major precipitation-producing cloud systems in GATE were mesoscale in extent, producing radar echoes up to 10^4 km^2 in area. These mesoscale cloud systems, moreover, had a complex internal structure with two distinct types of precipitation: *convective* (or cumulus)-scale vertically oriented cells of intense precipitation, ~1–10 km in horizontal dimension, and *mesoscale* (~100 km horizontal dimension) regions of horizontally stratified precipitation falling from thick anvil clouds emanating from the convective cells. Associated with the convective cells were convective-scale updrafts and downdrafts, evidently of the buoyant, nonhydrostatic type normally associated with cumuliform clouds, while more widespread mesoscale updrafts and downdrafts appeared to be associated with the anvil precipitation. The mesoscale updrafts and downdrafts have been produced in a numerical model by Brown (1979) and appear to be hydrostatic, the downdraft being driven by evaporation and melting of precipitation particles below the base of the anvil cloud. The mesoscale downdraft is of the type first described by Zipser (1969). The likely importance of the mesoscale vertical motions associated with anvil clouds is supported by the fact that ~40% of the rain in GATE can be attributed to anvils (Cheng and Houze, 1980).

There is a need now to translate these qualitative indications of the types of updrafts and downdrafts into quantitative determinations of the relative importance of the various scales of updrafts and down-

[1] Contribution No. 518, Department of Atmospheric Sciences, University of Washington.

[2] Present affiliation: Atmospheric Science Group, Texas Tech University, Lubbock 79409.

0022-4928/80/040754-20$09.00

drafts to large-scale atmospheric motions. To accomplish this task, carefully designed diagnostic methods are needed, as it is not observationally feasible to detect and measure the properties of each individual cloud updraft and downdraft in an ensemble of clouds within a region the size of a grid square in a large-scale numerical model. However, the *collective* effects of the cloud vertical motions on the large-scale environment can be determined from rawinsondes, raingages and weather radars. Properties of the clouds producing the collective effects can be diagnosed by using model clouds to represent the actual clouds in the population. The dynamic and thermodynamic properties of the model clouds are governed by equations for convective and mesoscale motions. By integrating over the population of model clouds, expressions for the collective effects of the clouds on their environment can be obtained. Substitution of the measured effects of real cloud populations into the expressions for the collective effects of the model cloud population makes it possible to solve for the dynamic and thermodynamic properties of the model clouds which produce the same large-scale effects as the real clouds. To the extent that the postulated model clouds are realistic, the properties of the real clouds are thus diagnosed.

The fact that the correctness of the diagnosed cloud properties depends on the realism of the postulated model clouds is a primary concern of this paper. We consider the two types of diagnostic methods that have been developed and used previously. One type, which we call the *synoptic approach*, uses the collective effects of the clouds on large-scale heat and moisture budgets derived from rawinsonde data as input (Yanai *et al.*, 1973; Ogura and Cho, 1973; Nitta, 1975, 1977; Johnson, 1976). The other type, which we call the *radar approach*, uses characteristics of observed precipitation patterns derived from weather radars and raingages as input (Austin and Houze, 1973; Lopez, 1973; Houze, 1973; Houze and Leary, 1976). These diagnostic approaches, as heretofore practiced, have the same shortcomings as current convective parameterization schemes, namely, the model clouds that they postulate are not very realistic in that they do not include all of the types of updrafts and downdrafts that appear to play a role in tropical convection. Johnson (1976), Houze and Leary (1976) and Nitta (1977) have considered convective-scale downdrafts in their diagnostic studies, and Johnson (1980) has recently included a form of mesoscale downdraft associated with anvils. However, none of these studies addresses the full problem of the uncertainty inherent in the diagnostic results as a result of the various types of model cloud populations that can be postulated.

In this paper, we make a start in this direction by developing a set of equations for a population of model clouds that have both convective and mesoscale vertical motions. The relative amounts of convective and mesoscale motion, which the model clouds are allowed to have, can be specified in these equations by adjusting certain model parameters. With such a set of equations, diagnostic calculations can be repeated with various combinations of the assumed parameters to measure the sensitivity of the diagnostic results to cloud model assumptions. One of the most important results of such sensitivity tests will be an assessment of the importance of taking into account mesoscale anvil air motions in the diagnosis and parameterization of convective cloud properties.

It is beyond the scope of the present paper to carry out all these sensitivity tests. Rather it is our present objective to provide the foundation for such tests by developing the necessary model. Subsequent papers (e.g., Cheng and Houze, 1980; Leary and Houze, 1980) will be concerned with the sensitivity testing. In developing the model in this paper we not only derive the basic equations (which are a straightforward extension of those used in previous diagnostic studies) and identify the cloud model assumptions that must be made to apply the model diagnostically, we also show that the same model can be applied in either the radar or synoptic approach. Consequently, if radar and synoptic input data are perfect, both approaches should lead to similar diagnostic results. We test this conclusion by performing a controlled experiment in which our model, with the same assumptions, is applied in both the radar and synoptic approaches using data from Phase III of GATE. This test shows that similar results can indeed be obtained using the model in either approach. To perform the test, however, we do not use the model in its most general form. We use a special case of the model in which its parameters are adjusted to make the model identical to that of Johnson (1976). In this form, the model's mesoscale updrafts and downdrafts are not activated. These drafts are activated in Leary and Houze (1980) and in future papers in which we test the sensitivity of diagnosed mass and heat fluxes to the inclusion of mesoscale motions in the model.

2. Model clouds used in diagnosing the properties of a population of clouds

a. General features of the model clouds

Model clouds simulating a population of real clouds in an area A are depicted schematically in Fig. 1. As in previous diagnostic studies of convective clouds,[3] it is assumed that the cloud population

[3] In the remainder of the paper, "previous diagnostic studies" refers primarily to Yanai *et al.* (1973), Ogura and Cho (1973), Austin and Houze (1973), Houze (1973), Nitta (1975, 1977), Houze and Leary (1976) and Johnson (1976, 1977).

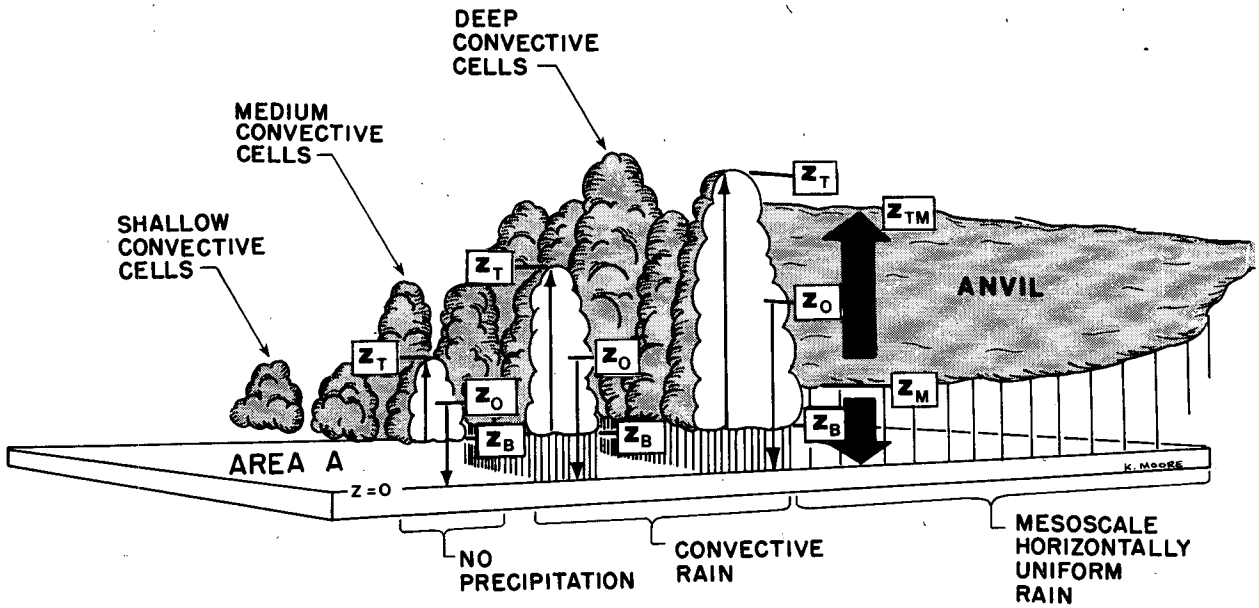

FIG. 1. Schematic of a typical population of clouds over a tropical ocean. Thin arrows represent convective-scale updrafts and downdrafts. Wide arrows represent mesoscale updrafts and downdrafts. Other details and symbols are described in the text.

contains convective cells ranging in size from shallow non-precipitating cells to medium-sized precipitating cells to deep precipitating cells. Following Houze and Leary (1976) and Johnson (1976, 1977), we assume that there is a *convective-scale updraft* and a *convective-scale downdraft* within each convective cell. We depart from previous studies, however, by further allowing the deep convective cells to have associated with them a widespread anvil cloud which can deposit large quantities of horizontally uniform rain over a mesoscale region. We assume that a *mesoscale updraft* of the type modeled by Brown (1979) may occur in the anvil cloud, between levels z_m and z_{Tm} in Fig. 1, and a *mesoscale downdraft* of the type described by Zipser (1969) and also modeled by Brown may occur below the base of the anvil cloud, between z_m and the surface ($z = 0$).

The population of model clouds shown in Fig. 1 is idealized in that it contains only one convective cell of each height and one anvil cloud, when actually there may be present any number of convective cells of a given height, and more than one precipitating anvil cloud. We assume that any two clouds of the same size and type have the same thermodynamic and dynamic properties. Therefore, a single bulk cloud can comprise all of the mass transport by updrafts and downdrafts in clouds of that particular type and size. Thus, a convective cell in Fig. 1 represents a bulk cell made up of all cells of the same height z_T, and the anvil cloud is a composite of all of the anvil clouds occurring in the cloud population.

The thermodynamic and dynamic properties of the convective and mesoscale updrafts and downdrafts of the model clouds illustrated in Fig. 1 are described in the following subsections. To make the description complete we indicate how the mesoscale vertical motions associated with anvil clouds are included in our ensemble of model clouds. As will be shown in Section 3, the amount of mesoscale motion allowed in the model ensemble is controlled by assumptions about cloud water budgets. The calculations of the controlled experiment described in Section 6 use a form of the general model depicted in Fig. 1 in which the mesoscale motions are set to zero by adjusting our model parameters to be consistent with Johnson (1976). In subsequent papers (e.g., Leary and Houze, 1980) we will readjust the model parameters to more realistic values which allow for non-zero mesoscale updraft and downdraft motions.

b. *Convective-scale updrafts*

As in previous diagnostic studies, the convective updrafts are modeled in a manner similar to that used in the cumulus parameterization scheme of Arakawa and Schubert (1974). It is assumed that the maximum height z_T reached by a convective-scale updraft is related uniquely to its entrainment rate λ by a function of the form

$$z_T = z_T(\lambda), \tag{1}$$

in which z_T increases monotonically with decreasing λ. The value of λ is constant with height z in a particular updraft. The total vertical mass flux through height z accomplished by all of the convective-scale updrafts that occur in area A during a period of time τ is given by

$$M_u(z) = (A\tau)^{-1} \int_0^{\lambda_T(z)} \mathcal{M}_u(\lambda,z)d\lambda, \quad (2)$$

where $\lambda_T(z)$ is the entrainment rate for convective clouds with tops at z_T and $\mathcal{M}_u(\lambda,z)d\lambda$ is the total mass of air transported through level z by convective-scale updrafts with entrainment rates between λ and $\lambda + d\lambda$.

The z variation of $\mathcal{M}_u(\lambda,z)$ can be expressed by a profile $f_u(\lambda,z)$, which is defined such that

$$\mathcal{M}_u(\lambda,z) = \mathcal{M}_B(\lambda)f_u(\lambda,z), \quad (3)$$

where $\mathcal{M}_B(\lambda) = \mathcal{M}_u(\lambda,z_B)$, z_B is the height of cloud base (assumed to be the same for all convective updrafts) and $f_u(\lambda,z_B)$ is unity for all λ.

The profile $f_u(\lambda,z)$ is related to the entrainment rate. The latter is defined as

$$\lambda = \frac{1}{\mathcal{M}_u(\lambda,z)}\left[\frac{\partial \mathcal{M}_u(\lambda,z)}{\partial z}\right]_\epsilon, \quad (4)$$

where the subscript ϵ indicates the part of the derivative due to entrainment. The total rate of change of $\mathcal{M}_u(\lambda,z)$ with z is given by

$$\frac{\partial \mathcal{M}_u(\lambda,z)}{\partial z} = \left[\frac{\partial \mathcal{M}_u(\lambda,z)}{\partial z}\right]_\epsilon + \left[\frac{\partial \mathcal{M}_u(\lambda,z)}{\partial z}\right]_\delta, \quad (5)$$

where the subscript δ indicates the change of $\mathcal{M}_u(\lambda,z)$ due to detrainment. Substituting (3) and (4) into (5) and rearranging terms, we see that the simultaneous specification of $f_u(\lambda,z)$ and λ [from (1)] implies a value for the detrainment rate given by

$$\frac{1}{\mathcal{M}_u(\lambda,z)}\left[\frac{\partial \mathcal{M}_u(\lambda,z)}{\partial z}\right]_\delta = \frac{1}{f_u}\frac{\partial f_u(\lambda,z)}{\partial z} - \lambda. \quad (6)$$

Since the detrainment rate cannot be a positive quantity, the prescribed profile $f_u(\lambda,z)$ must satisfy the condition

$$\frac{1}{f_u}\frac{\partial f_u(\lambda,z)}{\partial z} \leq \lambda. \quad (7)$$

Austin and Houze (1973) showed the range of possible profiles $f_u(\lambda,z)$ satisfying this condition and chose an intermediate one (see also Houze, 1973, and Houze and Leary, 1976). Other investigations (e.g., Yanai, *et al.*, 1973; Ogura and Cho, 1973; Johnson, 1976) chose to assume that the equality in (7) applies at all levels below cloud top. This assumption, according to (6), means physically that all detrainment occurs in an infinitesimally thin layer at cloud top. In a later paper, Johnson (1977) modified this assumption and considered profiles of $f_u(\lambda,z)$ similar to those of Austin and Houze (1973), which allowed some detrainment to occur below cloud top.

The value of a variable such as heat, moisture or momentum per unit mass of air at a given height in a convective-scale updraft is represented by $\xi_u(\lambda,z)$ and, following the convention of previous diagnostic studies, is assumed to be governed by the one-dimensional steady-state plume equation

$$\frac{\partial \xi_u(\lambda,z)}{\partial z} = \lambda[\hat{\xi}_u(z) - \xi_u(\lambda,z)] + S_u, \quad (8)$$

where $\hat{\xi}_u(z)$ is the value of ξ of the air entrained into the updraft from its surroundings and S_u stands for sources and sinks of $\xi_u(\lambda,z)$ other than entrainment. In most studies, the entrained air is assumed to come directly from the large-scale environment, in which case $\hat{\xi}_u(\lambda,z) = \xi_e(z)$, where the subscript e indicates properties of the large-scale environment. In (8), we allow, symbolically, for the possibility that the entrained air might be a mixture of cloud and environment air with $\hat{\xi}_u(\lambda,z) \neq \xi_e(z)$.

The moist static energy is defined as

$$h = c_pT + gz + Lq, \quad (9)$$

where c_p is the specific heat at constant pressure, T temperature, L the latent heat of vaporization and q the water-vapor mixing ratio. Since h is a conservative quantity (i.e., $S_u = 0$), we obtain

$$\frac{\partial h_u(\lambda,z)}{\partial z} = \lambda[\hat{h}_u(z) - h_u(\lambda,z)] \quad (10)$$

when h is substituted for ξ in (8). This first-order differential equation has the solution

$$h_u(\lambda,z) = h_u(z_B)e^{\lambda(z_B-z)} + \lambda e^{-\lambda z}\int_{z_B}^{z} e^{\lambda z'}\hat{h}_u(\lambda,z')dz'. \quad (11)$$

If an air parcel is saturated and its temperature is only slightly different from that of its large-scale environment at the same altitude, then a Taylor series expansion shows that its temperature $T(z)$ and mixing ratio $q(z)$ are related to its moist static energy $h(z)$ by the approximations

$$T(z) \approx T_e(z) + \frac{1}{c_p(1+\gamma)}[h(z) - h_e^*(z)], \quad (12)$$

$$q(z) \approx q_e(z) + \frac{1}{L}\left(\frac{\gamma}{1+\gamma}\right)[h(z) - h_e^*(z)], \quad (13)$$

where q^* is the saturation mixing ratio, $p(z)$ is the pressure at height z, $\gamma \equiv (L/c_p)[\partial q^*(T,p)/\partial T]_{T_e,p(z)}$, and the saturation moist-static energy h^* is defined as $c_pT + qz + Lq^*$.

Since convective-scale updrafts are saturated, we use (12) and (13) to calculate the updraft temperature $T_u(\lambda,z)$ and water-vapor mixing ratio $q_u(\lambda,z)$ from the value of $h_u(\lambda,z)$ computed in (11).

c. Convective-scale downdrafts

Following Houze and Leary (1976) and Johnson (1976)[4], we assume that the convective-scale updraft in each of our model convective cells (Fig. 1) is accompanied by a convective-scale downdraft which has the same fractional entrainment rate λ as the updraft. The downdrafts, then, are modeled as inverted updrafts with

$$\lambda = -\frac{1}{\mathcal{M}_d(\lambda,z)}\left[\frac{\partial \mathcal{M}_d(\lambda,z)}{\partial z}\right]_\epsilon, \tag{14}$$

where $\mathcal{M}_d(\lambda,z)d\lambda$ is the total mass transport (negative) through level z by convective-scale downdrafts in clouds with entrainment rates between λ and $\lambda + d\lambda$, and $[\partial \mathcal{M}_d(\lambda,z)/\partial z)]_\epsilon$ is the rate of change of $\mathcal{M}_d(\lambda,z)$ with z due to entrainment. A relation analogous to (5) for downdrafts is

$$\frac{\partial \mathcal{M}_d(\lambda,z)}{\partial z} = \left[\frac{\partial \mathcal{M}_d(\lambda,z)}{\partial z}\right]_\epsilon + \left[\frac{\partial \mathcal{M}_d(\lambda,z)}{\partial z}\right]_\delta, \tag{15}$$

where the second term on the right-hand side is the contribution to $\partial \mathcal{M}(\lambda,z)/\partial z$ due to detrainment.

It is assumed that the downdrafts originate at some level z_0 below cloud top z_T (Fig. 1). Since $z_0 \leq z_T$, the total vertical mass flux through height z accomplished by all of the convective-scale downdrafts in area A during time τ can be written as

$$M_d(z) = (A\tau)^{-1}\int_0^{\lambda_T(z)} \mathcal{M}_d(\lambda,z)d\lambda. \tag{16}$$

The z variation of $\mathcal{M}_d(\lambda,z)$ is prescribed in the form of a profile $f_d(\lambda,z)$ such that

$$\mathcal{M}_d(\lambda,z) = \mathcal{M}_0(\lambda)f_d(\lambda,z), \tag{17}$$

where $\mathcal{M}_0(\lambda) = \mathcal{M}_d(\lambda,z_0)$, $f_d(\lambda,z_0) = 1$ and $f_d(\lambda,z) > 1$ for $z < z_0$.

Following Johnson (1976) and Houze and Leary (1976), we further assume that the strength of the convective-scale downdrafts in convective cells of a given size (or λ) is related to the strength of the convective-scale updrafts by a function of the form

$$\mathcal{M}_0(\lambda) = f[\mathcal{M}_B(\lambda)]. \tag{18}$$

It will be shown in a subsequent section that $\mathcal{M}_0$ is related to $\mathcal{M}_B(\lambda)$ through the water budget of the model clouds.

The average value of a variable such as heat, moisture or momentum per unit mass at a given height within a convective-scale downdraft is represented by $\xi_d(\lambda,z)$ and is governed by an expression similar to (8), *viz.*,

[4] An approach such as Nitta's (1977) leads only to bulk downdraft properties, whereas we prefer to deal with spectrally decomposed properties which can be related to a radar-observed spectrum of precipitation.

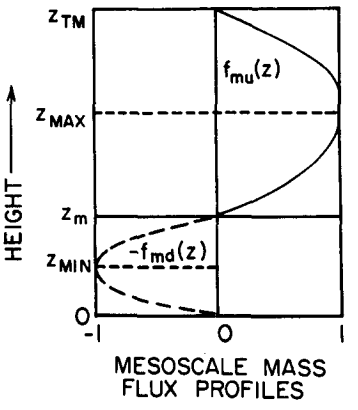

FIG. 2. Schematic illustration of the mass flux profiles for the mesoscale updraft (f_{mu}) and downdraft (f_{md}) in the bulk anvil cloud.

$$\frac{\partial \xi_d(\lambda,z)}{\partial z} = -\lambda[\hat{\xi}_d(z) - \xi_d(\lambda,z)] + S_d, \tag{19}$$

where $\xi_d(z)$ is the value of ξ of the air entrained into the downdraft and S_d includes any sources or sinks of $\xi_d(\lambda,z)$ other than entrainment. The equation for the moist-static energy in the convective-scale downdraft obtained as a special case of (19), similar to (9), is

$$\frac{\partial h_d(\lambda,z)}{\partial z} = -\lambda[\hat{h}_d(z) - h_d(\lambda,z)], \tag{20}$$

which has the solution

$$h_d(\lambda,z) = h_d(z_0)e^{-\lambda(z_0-z)} - \lambda e^{\lambda z}\int_{z_0}^{z} e^{-\lambda z'}\hat{h}_d(\lambda,z')dz'. \tag{21}$$

Following Johnson (1976) and Houze and Leary (1976), we assume that convective-scale downdrafts are saturated and compute their temperature $T_d(\lambda,z)$ and mixing ratio $q_d(\lambda,z)$ from (12) and (13). Recently, Betts and Silva Dias (1979) have suggested the use of a parametric formula for computing the rate of evaporation of raindrops in a downdraft. According to this formula, downdrafts can be found to be slightly subsaturated. We do not believe, however, that the inclusion of this refinement in our calculations would significantly alter our results.

d. Mesoscale vertical motions

The contribution to the total vertical mass flux in area A during time τ by the mesoscale air motions associated with the anvil cloud depicted in Fig. 1 may be expressed as

$$M_m(z) = \frac{\mu_m(z)}{A\tau}, \tag{22}$$

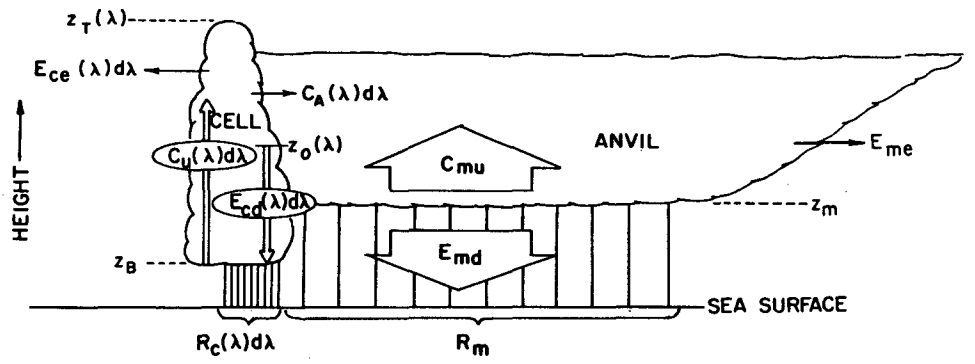

FIG. 3. Schematic showing the water budget parameters for one category of convective cell interacting with the bulk anvil cloud. The narrow upward arrow represents the convective updraft associated with condensation in the cell $C_u(\lambda)d\lambda$. The narrow downward arrow represents the convective downdraft associated with evaporation in the cell $E_{cd}(\lambda)d\lambda$. The wide upward arrow represents the mesoscale updraft associated with the condensation in the anvil C_{mu}. The wide downward arrow represents the mesoscale downdraft associated with the evaporation under the anvil E_{md}. Horizontal arrows represent condensate from the cell $[E_{ce}(\lambda)d\lambda]$ and the anvil (E_{me}) that evaporates in the large-scale environment and condensate from the cell that is incorporated into the anvil $[C_A(\lambda)d\lambda]$. $R_c(\lambda)d\lambda$ and R_m are the rainfall from the cell and the anvil, respectively. Other symbols are defined in the text.

where

$$\mu_m(z) = \begin{cases} \mu_{mu}(z), & z_m \leq z \leq z_{Tm} \\ \mu_{md}(z), & 0 \leq z \leq z_m \end{cases} \tag{23}$$

and $\mu_{mu}(z)$ (a positive quantity) and $\mu_{md}(z)$ (a negative quantity) are the total amounts of mass transported through level z in the mesoscale updraft and downdraft, respectively. The z variation of $\mu_m(z)$ may be expressed in terms of the profiles $f_{mu}(z)$ and $f_{md}(z)$ illustrated schematically in Fig. 2. The functional forms of these profiles in a particular set of diagnostic calculations have to be prescribed. The profiles are defined such that

$$\mu_{mu}(z) = \mu^*_{mu} f_{mu}(z), \tag{24}$$

$$\mu_{md}(z) = \mu^*_{md} f_{md}(z), \tag{25}$$

where $\mu^*_{mu} \equiv \mu_{mu}(z_{MAX})$ and $\mu^*_{md} = \mu_{md}(z_{MIN})$. The levels z_{MAX} and z_{MIN} are the heights at which $f_{mu}(z)$ and $f_{md}(z)$ have their maximum values of unity, while at levels z_m and z_{Tm}, the base and top of the mesoscale updraft, respectively, $f_{mu}(z)$ is zero, and at levels $z = 0$ and z_m, the base and top of the mesoscale downdraft, respectively, $f_{md}(z)$ is zero.

For variables such as heat, moisture or momentum per unit mass of air, we let the subscript m represent an average over the lifetime and area covered by the bulk anvil cloud depicted in Fig. 1. This average, for an arbitrary quantity ξ, is governed by the equation

$$\frac{d\xi_m}{dz} = \left[\frac{\partial \xi(x,y,z,t)}{\partial z}\right]_m = S_m - \mathcal{S}_m - \mathcal{H}_m, \tag{26}$$

where x and y are horizontal coordinates, t is time, S_m represents sources and sinks of $\xi_m(z)$, $\mathcal{S}_m$ is the effect of storage given by

$$\mathcal{S}_m = w_m^{-1}\left[\frac{\partial \xi(x,y,z,t)}{\partial t}\right]_m, \tag{27}$$

where w_m is the vertical velocity averaged over the lifetime and area covered by the anvil cloud, and $\mathcal{H}_m$ is the effect of horizontal advection, given by

$$\mathcal{H}_m = \frac{(\mathbf{V}_R)_m \cdot (\nabla \xi)_m}{w_m}, \tag{28}$$

where $\mathbf{V}_R$ is the horizontal wind relative to the anvil cloud.

Eq. (26) is the mesoscale analog of (8) and (19). It can be used to calculate the moist static energy, temperature (or dry static energy) and water vapor mixing ratio in anvil clouds. More details will be given in subsequent papers dealing with the sensitivity of the diagnostic results to anvil air motions (e.g., Leary and Houze, 1980).

3. Water budget of a population of model clouds

We consider now the water budget of the population of model clouds pictured in Fig. 1. In this population, water can be condensed either in the convective-scale updrafts of the cells of various heights or in the mesoscale updraft of the anvil cloud.

a. Condensation in convective cells

The mass of water condensed in the convective-scale updrafts of cells with entrainment rates between λ and $\lambda + d\lambda$ is given by $C_u(\lambda)d\lambda$, where

$$C_u(\lambda)d\lambda = \int_{z_B}^{z_T(\lambda)} \mathcal{M}_u(\lambda,z)d\lambda\left[\lambda(\hat{q}_u - q_u) - \frac{\partial q_u}{\partial z}\right]dz. \quad (29)$$

As shown by Austin and Houze (1973), this equation is obtained by letting $\xi = q$ in an equation of the form (8) and then integrating from cloud base z_B to cloud top $z_T(\lambda)$.

The condensate given by (29) is apportioned according to

$$C_u(\lambda)d\lambda = [R_c(\lambda) + E_{cd}(\lambda) + E_{ce}(\lambda) + C_A(\lambda)]d\lambda, \quad (30)$$

where $R_c(\lambda)d\lambda$ falls as precipitation, $E_{cd}(\lambda)d\lambda$ and $E_{ce}(\lambda)d\lambda$ are the portions of the condensate $C_u(\lambda)d\lambda$ which are reevaporated in convective-scale downdrafts and in the large-scale environment, respectively; and $C_A(\lambda)d\lambda$ is the portion of $C_u(\lambda)d\lambda$ which is incorporated into the mesoscale region covered by the anvil cloud, either by being detrained, that is, carried horizontally into the anvil region by air flowing out of convective cells, or by being left aloft by dying cells, which upon ending their periods as active convective entities, blend into the anvil cloud while new cells form ahead of the anvil region (Houze, 1977; Leary and Houze, 1979b). The water budget expressed by (30) is illustrated schematically in Fig. 3. Expressing the four terms on the right-hand side of (30) as fractions of $C_u(\lambda)d\lambda$, we obtain

$$R_c(\lambda)d\lambda = \nu_c(\lambda)C_u(\lambda)d\lambda, \quad (31)$$

$$E_{cd}(\lambda)d\lambda = \alpha(\lambda)C_u(\lambda)d\lambda, \quad (32)$$

$$E_{ce}(\lambda)d\lambda = \beta(\lambda)C_u(\lambda)d\lambda, \quad (33)$$

$$C_A(\lambda)d\lambda = \eta(\lambda)C_u(\lambda)d\lambda, \quad (34)$$

where $\nu_c(\lambda)$, $\alpha(\lambda)$, $\beta(\lambda)$ and $\eta(\lambda)$ are each either zero or a positive fraction. To be consistent with (30), they must satisfy the constraint that

$$\nu_c(\lambda) + \alpha(\lambda) + \beta(\lambda) + \eta(\lambda) = 1. \quad (35)$$

It may appear that to represent the water budget, we are introducing more arbitrary parameters (such as α, β, η and ν_c) than have been involved in previous diagnostic models. However, we are not really introducing these parameters for the first time, but rather recognizing them perhaps more openly. In previous studies the same parameters are involved but have usually been tacitly adjusted to be consistent with an assumption of the absence of mesoscale motions, as will be shown below in Section 5c.

The quantity $\nu_c(\lambda)$ is of particular significance as it is the efficiency with which the condensate produced in the convective-scale updrafts of cells with entrainment rates from λ to $\lambda + d\lambda$ is converted to convective precipitation. For precipitating cells, $\nu_c(\lambda) > 0$, and Eqs. (3) and (31) may then be used to rewrite (29) as

$$\frac{R_c(\lambda)d\lambda}{\nu_c(\lambda)} = I_1(\lambda)\mathcal{M}_B(\lambda)d\lambda, \quad (36)$$

where

$$I_1(\lambda) = \int_{z_B}^{z_T(\lambda)} f_u(\lambda,z)\left[\lambda(\hat{q}_u - q_u) - \frac{\partial q_u(\lambda,z)}{\partial z}\right]dz. \quad (37)$$

If a relationship between cell height z_T and entrainment rate λ is provided [Eq. (1)], a profile $f_u(\lambda,z)$ is prescribed, the mixing ratio $\hat{q}_u(\lambda,z)$ of the entrained air is known and $\partial q_u/\partial z$ is computed from an equation of the form (8), then the integral $I_1(\lambda)$ can be evaluated. If, furthermore, the amount of rain $R_c(\lambda)d\lambda$ which falls from cells with entrainment rates in the interval λ to $\lambda + d\lambda$ is measured, and an appropriate efficiency $\nu_c(\lambda)$ is assumed, then the cloud-base mass transport $\mathcal{M}_B(\lambda)d\lambda$ can be determined from (36). Such a procedure constitutes Austin and Houze's (1973) method of diagnosing the mass transports of precipitating convective clouds.

b. *Evaporation in convective downdrafts*

Through expressions analogous to (29) and (36), the evaporation of moisture in the convective-scale downdrafts of cells with entrainment rates between λ and $\lambda + d\lambda$ is given by

$$E_{cd}(\lambda)d\lambda = I_2(\lambda)\mathcal{M}_0(\lambda)d\lambda, \quad (38)$$

where we have made use of (17) and the definition

$$I_2(\lambda) = \int_0^{z_0} f_d(\lambda,z)\left[\lambda(\hat{q}_d - q_d) + \frac{\partial q_d(\lambda,z)}{\partial z}\right]dz. \quad (39)$$

But from (31) and (36), we have

$$E_{cd}(\lambda)d\lambda = \alpha(\lambda)C_u(\lambda)d\lambda = \alpha(\lambda)I_1(\lambda)\mathcal{M}_B(\lambda)d\lambda. \quad (40)$$

Equating the right-hand sides of (38) and (40) and rearranging terms, we obtain

$$\mathcal{M}_0(\lambda) = \epsilon(\lambda)\mathcal{M}_B(\lambda), \quad (41)$$

where

$$\epsilon(\lambda) = \frac{\alpha(\lambda)I_1(\lambda)}{I_2(\lambda)}. \quad (42)$$

The relationships (41) and (42) give a specific form to Eq. (18) which relates the downdraft mass transport parameter $\mathcal{M}_0(\lambda)$ to the updraft mass transport parameter $\mathcal{M}_B(\lambda)$ for cells of a given size $z_T(\lambda)$. From (32), (41) and (42), it is clear that $\mathcal{M}_0(\lambda)$ and $\mathcal{M}_B(\lambda)$ are related to each other through the water budget of convective cells and that the proportionality factor $\epsilon(\lambda)$ is primarily an expression of the reevaporation of convective condensate in convective-scale downdrafts. Houze and Leary (1976), with different

notation, used (41) and (42) in computing downdraft mass transports in an extension of Austin and Houze's (1973) diagnostic method. Johnson (1976) introduced the notation $\epsilon(\lambda)$, but simply assigned $\epsilon(\lambda)$ a number rather than expressing it physically in terms of $\alpha(\lambda)$, $I_1(\lambda)$ and $I_2(\lambda)$. For guidance in making assumptions in diagnostic calculations, it may be easier to relate studies of cloud water budgets to the physically simple parameter $\alpha(\lambda)$ than the more physically complex quantity $\epsilon(\lambda)$.

c. Condensation in anvil clouds

The mass of water condensed in the mesoscale updraft of the bulk anvil cloud depicted in Fig. 1 can be expressed by

$$C_{mu} = -\int_{z_m}^{z_{Tm}} \mu_{mu}(z)\frac{dq_m}{dz}\,dz. \tag{43}$$

This equation is obtained by letting $\xi = q$ in (26) and assuming that the sink of water vapor due to condensation is the only significant term determining the value of dq_m/dz in that equation. That is, there is assumed to be an approximate balance between condensation and vertical advection of water vapor in the anvil cloud.

The mesoscale anvil cloud can consist partly of water condensed in its adjoining convective cells and introduced into the anvil through the effects represented by $C_A(\lambda)d\lambda$ in (30) and partly of the condensate C_{mu} generated by lifting within the anvil cloud itself. Thus, we have

$$C_{mu} + C_A^* = R_m + E_{md} + E_{me}, \tag{44}$$

where

$$C_A^* = \int_0^\infty C_A(\lambda)d\lambda, \tag{45}$$

R_m is the total mass of mesoscale horizontally uniform rain which falls from the anvil cloud, E_{md} the portion of $(C_{mu} + C_A^*)$ which is reevaporated in the mesoscale downdraft below the base of the anvil cloud, and E_{me} the portion of $(C_{mu} + C_A^*)$ which is detrained or left aloft by the anvil cloud to be reevaporated in the large-scale environment. The water budget expressed by (44) is illustrated schematically in Fig. 3. Expressing the terms on the right-hand side of (44) as fractions of $(C_{mu} + C_A^*)$, we obtain

$$R_m = \nu_m(C_{mu} + C_A^*), \tag{46}$$

$$E_{md} = a(C_{mu} + C_A^*), \tag{47}$$

$$E_{me} = b(C_{mu} + C_A^*), \tag{48}$$

where ν_m, a and b are zero or positive fractions which, to be consistent with (44), must satisfy the constraint that

$$\nu_m + a + b = 1. \tag{49}$$

The term ν_m is the efficiency with which condensate in the anvil cloud is converted to mesoscale precipitation (R_m).

Limits on the amount of mesoscale lifting which occurs in the anvil region of the model cloud population can be determined by rewriting Eq. (43), after substitution from (24), as

$$\mu_{mu}^* = \frac{C_{mu}}{I_3}, \tag{50}$$

where

$$I_3 = -\int_{z_m}^{z_{Tm}} f_{mu}(z)\frac{dq_m}{dz}\,dz. \tag{51}$$

Eq. (50) gives a specific formula for computing μ_{mu}^*, which, in (24), is the parameter that expresses the magnitude of the mass transport by the mesoscale updraft in the anvil cloud.

Two extreme cases can be identified in examining Eqs. (44) and (50). Either

$$\text{(a)}\quad C_A^* = 0 \tag{52}$$

or

$$\text{(b)}\quad C_{mu} = 0. \tag{53}$$

In Case (a), C_{mu} is a maximum according to (44). Since $C_A^* = 0$, no condensate is transferred into the anvil region from convective cells. Hence, lifting in the anvil must produce enough condensate to explain all of $R_m + E_{md} + E_{me}$. Consequently, μ_{mu}^* is a maximum in this case.

In Case (b), μ_{mu}^* is zero according to (50). Since $C_{mu} = 0$, all of the observed mesoscale rain is accounted for, according to (44), by the transfer of condensate C_A^*, into the anvil region from adjacent convective cells. Consequently, there is no need for any lifting to occur in the anvil region.

Again, we are not really introducing new parameters [e.g., ν_m, $f_{mu}(z)$, z_m, thermodynamic conditions at z_m] into our diagnostic model in order to include a mesoscale updraft. Previous studies, rather, have avoided dealing with such parameters explicitly by making the tacit assumption of Case (b) (See Section 5c for further discussion). In the diagnostic calculations presented in this paper we follow the traditional practice of assuming Case (b). In subsequent papers [such as Leary and Houze (1980)] we will test the sensitivity of diagnostic results to the presence of mesoscale updrafts by considering a range of values of C_{mu} lying between those of Cases (a) and (b).

d. Evaporation below anvil clouds

The evaporation of water in the mesoscale downdraft (E_{md}) may be expressed, using (25), in an equation analogous to (43), *viz.*,

$$E_{md} = \mu_{md}^* I_4, \tag{54}$$

where

$$I_4 = \int_0^{z_m} f_{md}(z) \frac{dq_m}{dz} dz. \quad (55)$$

Substitution of (47) and (46) into (54) leads to

$$\mu^*_{md} = \frac{a(C_{mu} + C^*_A)}{I_4} = \frac{aR_m}{I_4 \nu_m}, \quad (56)$$

where the last expression applies only if ν_m is nonzero. According to (56), μ^*_{md} depends on the sum $(C_{mu} + C^*_A)$, whereas, according to (50), μ^*_{mu}, the mesoscale updraft parameter, depends only on C_{mu}. It follows that a mesoscale downdraft can exist in the absence of a mesoscale updraft ($C_{mu} = 0$), provided C^*_A is nonzero. This result is reasonable since the amount of evaporation that can take place in the mesoscale downdraft depends only on the amount of precipitation that *falls out* of the anvil cloud into the layer below. It does not depend on where or how the evaporating precipitation particles were generated. The strength of the mesoscale updraft, on the other hand, is related entirely to how much condensation takes place in the anvil itself.

As for the mesoscale updraft, we are not really introducing new parameters [a, f_{md}, z_m, thermodynamic conditions at z_m] in order to represent the mesoscale downdraft. In the past, these parameters have been avoided by tacitly setting $a = 0$. In the present paper, we follow the traditional procedure of assuming that no mesoscale downdrafts occurred by setting $a = 0$ in (56). In subsequent papers, we will test the sensitivity of diagnostic results to the presence of mesoscale downdrafts by considering values of a lying between 0 and 1.

4. Heat flux by the population of model clouds

The vertical eddy flux of moist static energy (which we call the heat flux) for a simple situation in which one convective cell and one anvil cloud exist in area A, in the absence of density variations, is

$$\overline{w'h'} = \sigma_u w_u(h_u - h_e) + \sigma_d w_d(h_d - h_e) + \sigma_m w_m(h_m - h_e) - \bar{w}\sigma_u(h_u - h_e) - \bar{w}\sigma_d(h_d - h_e) - \bar{w}\sigma_m(h_m - h_e), \quad (57)$$

where the overbar indicates an average over A, the prime is a deviation from such an average, σ_u, σ_d and σ_m are the fractions of area A covered by the updraft of the convective cell, the downdraft of the convective cell and the mesoscale anvil cloud, respectively, and w is the vertical velocity. Since the area covered by the convective cell is small compared with A, σ_u and σ_d are $\ll 1$, (57) becomes

$$\overline{w'h'} = \sigma_u w_u(h_u - h_e) + \sigma_d w_d(h_d - h_e) + \sigma_m w_m(h_m - h_e) - \bar{w}\sigma_m(h_m - h_e). \quad (58)$$

Since the anvil may cover a sizeable portion of A, the last term cannot be readily neglected on the basis of its areal coverage. However, if $w_m \approx 10$ cm s^{-1}, as suggested by Brown's (1979) model and Zipser's (1969, 1977) work, and $\bar{w} \approx 1$ cm s^{-1} as suggested by the work of Thompson *et al.* (1979), then the last term on the right-hand side of (58) may be negligible compared to the third term. For now, we retain the term for completeness. A generalized and time-averaged form of (58) for the entire population of clouds in Fig. 1 is

$$-\widetilde{\overline{\omega'h'}} = \frac{g}{A\tau} \int_0^{\lambda_T(p)} \{\mathcal{M}_u(\lambda,p)[h_u(\lambda,p) - \tilde{h}_e(p)] + \mathcal{M}_d(\lambda,p)[h_d(\lambda,p) - \tilde{h}_e(p)]\} d\lambda + \left[\frac{g\mu_m(p)}{A\tau} + \widetilde{\sigma_m\overline{\omega(p)}}\right][h_m(p) - \tilde{h}_e(p)], \quad (59)$$

where p is the pressure at height z, $\omega \equiv dp/dt$, g the gravitational acceleration and the tilde indicates an average over the time period τ. To obtain (59), it is assumed that differences between cloud and environment values of h do not vary with time during τ and can be represented by $[h - \tilde{h}_e(p)]$.

The heating due to the vertical convergence of the heat flux $-\overline{w'h'}$, obtained by taking the derivative of (59) with respect to p, is of the form

$$-\frac{\partial\widetilde{\overline{\omega'h'}}}{\partial p} = f_1(p) + \mathcal{M}_B(\lambda_T)f_2(p) + \int_0^{\lambda_T(p)} \mathcal{M}_B(\lambda)f_3(\lambda,p)d\lambda. \quad (60)$$

The derivation of this expression and explicit formulas for $f_1(p)$, $f_2(p)$ and $f_3(\lambda,p)$ are given in Appendix A.

This integral equation is a generalized version of Eq. (9) in Johnson (1977). It can be solved numerically for $\mathcal{M}_B(\lambda)$, provided that $-\partial\widetilde{\overline{\omega'h'}}/\partial p$ is known from heat and moisture budget studies and that the functions $f_1(p)$, $f_2(p)$ and $f_3(p)$ are either known or assumed. Thus, Eq. (60) provides another method, besides Austin and Houze's [based on Eq. (36)] for determining $\mathcal{M}_B(\lambda)$.

Johnson (1976) assumed that his cloud population contained no mesoscale anvil clouds. He further assumed that the air entrained into the convective cells had the properties of the large-scale environment, i.e., $\hat{h}_u(\lambda,p) = \hat{h}_d(\lambda,p) = \hat{h}_e(p)$, and that detrainment occurred only at the tops of updrafts and at the bottom (below cloud base) of downdrafts. Under these conditions, (60) reduces to

$$-\frac{\partial\widetilde{\overline{\omega' h'}}}{\partial p} = \frac{g}{A\tau}\left\{\delta^*(p)[h_u(\lambda_T,p) - \tilde{h}_e(p)] - \frac{\partial\tilde{h}_e}{\partial p}(M_u - M_d)\right\}, \quad (61)$$

where δ^* is defined in Appendix A. This equation is a time-averaged version of Eq. (24) of Johnson (1976). Eq. (9) of Johnson (1977) is also a special case of (60).

Physically, Eq. (61) indicates that the heating due to the vertical convergence of the vertical eddy flux of moist-static energy is manifested as a combination of both detrainment of excess moist-static energy from the tops of convective updrafts and vertical advection of environmental moist-static energy by the compensating downward motion outside of the cells. Physical processes which are ignored in (61), but included in (60) and (A1), are detrainment from the sides of convective-scale updrafts and downdrafts [terms involving $\delta_u(p)$ and $\delta_d(p)$ in (A1)], modification of environment air before it is entrained into convective-scale updrafts and downdrafts [terms involving $\hat{h}_u(\lambda,p)$ and $\hat{h}_d(\lambda,p)$], and the vertical convergence of the eddy flux of moist-static energy on the mesoscale (terms involving the subscript m).

5. Procedure for making diagnostic calculations and comparisons

a. Two approaches

As noted in the Introduction, two approaches may be used in diagnosing the properties of an ensemble of clouds: a *synoptic approach* and a *radar approach*. The synoptic approach uses methods such as those of Johnson (1976) to solve an equation of the form of (60) or (61) for the cloud base mass transport spectral function $\mathcal{M}_B(\lambda)$, given the total eddy heating $(-\partial\widetilde{\overline{\omega' h'}}/\partial p)$ derived from large-scale budget studies based on rawinsonde and radiation data. The radar approach, which uses methods similar to those of Austin and Houze (1973) and Houze and Leary (1976) is based on solving equations of the form of (36) for $\mathcal{M}_B(\lambda)$ and (50) and (56) for the mesoscale updraft and downdraft parameters μ^*_{mu} and μ^*_{md}, given radar measurements of the heights of convective cells (z_T), and the rainfall associated with the cells in each height category $[R_c(\lambda)d\lambda]$, and the precipitation from anvil clouds (R_m).

b. Assumptions

To obtain solutions for $\mathcal{M}_B(\lambda)$ by *either* approach, all of the following assumptions or provisions must be made, either explicitly or implicitly:

(i) The relationship between convective cell height z_T and entrainment rate in (1) must be given a specific form.

(ii) The heights z_B, the base of the convective updrafts, z_0, the top of the convective downdrafts and the boundary z_m between the mesoscale updraft and downdraft, must be specified.

(iii) The mass transport profiles $f_u(\lambda,z)$, $f_d(\lambda,z)$, $f_{mu}(z)$ and $f_{md}(z)$ must be prescribed.

(iv) The moist static energy of the air entrained into convective-scale updrafts and downdrafts, $\hat{h}_u(z)$ and $\hat{h}_d(z)$, must be determined.

(v) Boundary conditions for in-cloud temperature and water vapor mixing ratio must be assumed for level z_B in the convective-scale updrafts, level z_0 in the convective scale downdrafts and level z_m in the mesoscale updraft and downdraft.

(vi) A value for the quantity $\sigma_m\widetilde{\overline{\omega(p)}}$ in (59) must be assumed or provided by observation.

(vii) Three of the convective water budget parameters, $\nu_c(\lambda)$, $\alpha(\lambda)$, $\beta(\lambda)$ and $\eta(\lambda)$, and two of the mesoscale water budget parameters, ν_m, a and b, must be assumed.

c. Treatment of assumptions (i)–(vii) in the controlled experiment

In this paper, we perform a controlled experiment in which the above assumptions are treated in a similar way in both the synoptic and radar approaches. Differences in the results of the two approaches can then be attributed to differences in the independent data sets on which the calculations are based rather than to differences in model assumptions. For the synoptic approach we follow Johnson (1976), and, in the radar approach we treat assumptions (i)–(vii) just as he does. Details are described below.

ASSUMPTION (i)

Following, Johnson (1976), the convective cell height $z_T(\lambda)$ is based on a calculation of the level of zero buoyancy $z^*(\lambda)$. This is the level at which the cloud virtual temperature of the convective updraft in a cell of a given entrainment rate λ equals the virtual temperature of the environment, or the moist-static energy in the updraft $h_u(\lambda,z_T)$, computed from (11), has the value given by the right-hand side of Eq. (15) of Johnson (1976). Unfortunately, the function $z^*(\lambda)$ determined in this way from the GATE Phase III mean sounding of Thompson *et al.* (1979) (solid curve in Fig. 4) is double-valued between 750 and 600 mb, and hence its inverse cannot be used for $\lambda_T(p)$ in (60) or (61). To make the synoptic approach tractable we smoothed the entrainment function to obtain the monotonic function $z^*_s(\lambda)$ (dashed line in Fig. 4). This smoothing has almost no effect

on our results since we are concerned only with precipitating cells. In the radar approach, the input data show very little precipitation from cells with tops below 600 mb (~4.4 km) [Cheng and Houze's (1979) Fig. 2d; also see Sections 4d and 4e below]. In the synoptic approach, we use only the portion of the solution of (61) that applies above the 600 mb level. Since this solution is obtained by integrating downward, the portion of the solution above 600 mb is unaffected by the shape of the curve in Fig. 4 below 600 mb. If the full solution of (61) is used, then more caution is required in dealing with the cloud top-entrainment rate relationship (Johnson, 1979).

In the synoptic approach, the cell height is not actually observed. It is simply assumed to be the (in our case smoothed) level of zero buoyancy, that is $z_T(\lambda)$ is equated with $z_s^*(\lambda)$ in Fig. 4. In the radar approach, the cell height is an observed quantity. In GATE, the observed cell heights often exceeded the largest value of $z_s^*(\lambda)$ in Fig. 4 (~12 km). Cells < 12 km in maximum height are assigned values of λ by equating the observed z_T with the function $z_s^*(\lambda)$, as in the synoptic approach. Cells exceeding 12 km in height are arbitrarily assigned the same entrainment rate as a 12 km cell. A shortcoming of the synoptic approach is its inability to diagnose the presence of these deeper, overshooting convective cells.

ASSUMPTION (ii)

Convective updraft base z_B is assumed to be 558 m (the height of the 950 mb level in the mean GATE Phase III sounding) for cells of all heights. The top of the downdraft z_0 in cells of height z_T is assumed to be at the level where the pressure is $p(z_B) - 0.5[p(z_B) - p(z_T)]$. Since there are assumed to be no mesoscale updrafts or downdrafts, the value of z_m is immaterial.

ASSUMPTION (iii)

The profiles $f_u(\lambda,z)$ and $f_d(\lambda,z)$ are prescribed to be exponential by the assumption that the detrainment terms in (6) and (15) are zero except at the top of the convective-scale updraft and the bottom of the convective-scale downdraft. The mesoscale updraft and downdraft profiles $f_{mu}(z)$ and $f_{md}(z)$ are not needed because of assumption (vii).

ASSUMPTION (iv)

The entrained air is assumed to be characterized by the moist-static energy of the large-scale environment, so that

$$\hat{h}_u(z) = \hat{h}_d(z) = \tilde{\hat{h}}_e(z). \tag{62}$$

ASSUMPTION (v)

The air at the base of the convective updrafts z_B is assumed to have a virtual temperature excess of zero.[5] At the top of the convective downdrafts, z_0, the air is assumed to be saturated with a temperature excess of zero. Conditions at level z_m are irrelevant for the controlled experiment since, according to assumption (vii), there are assumed to be no mesoscale updrafts or downdrafts.

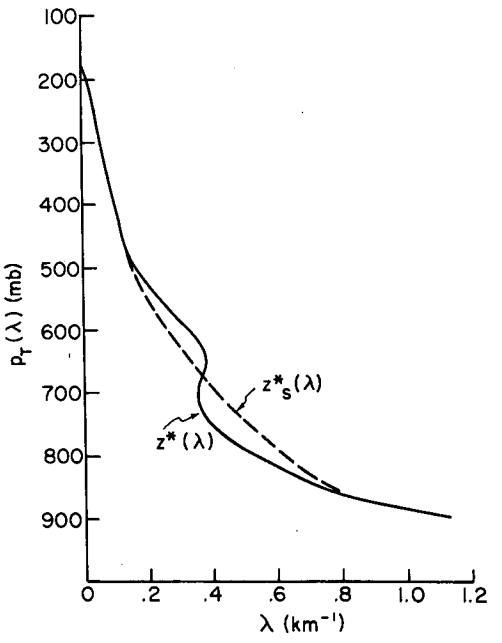

FIG. 4. Relationship between entrainment rate (λ) and pressure at cell top (p_T). See text for explanation.

ASSUMPTION (vi)

The term involving $\widetilde{\sigma_m\tilde{\omega}(p)}$ in (59) and (A1) is neglected.

ASSUMPTION (vii)

For the mesoscale anvil water budget, the parameter a is assumed to be zero. From (47), this implies that

$$E_{md} = 0. \tag{63}$$

The parameter ν_m is not assigned an explicit value, but is assumed to be given by R_m/C_A^*, which, from (46), implies that

$$C_{mu} = 0 \tag{64}$$

[case (b), Eq. (53)]. These assumptions force the diagnosed anvil updrafts and downdrafts to be zero according to (50) and (56). Physically, it is being assumed that the anvil rain R_m is all derived from condensate C_A^*, which is generated in the updrafts of convective cells, and that the anvil rain falls to the sea surface without any evaporation below the base of the anvil cloud.

[5] This assumption was discussed and used by Nitta (1975) as well as by Johnson (1976).

For the water budgets of the convective cells, the three parameters $\alpha(\lambda)$, $\nu_c(\lambda)$ and $\eta(\lambda)$ are specified. Following Johnson (1976), we specify them indirectly. The parameter $\alpha(\lambda)$ is prescribed by assigning a value to the parameter $\epsilon(\lambda)$ in (42). The value assigned to $\epsilon(\lambda)$ is assumed to be a constant, the value of which is determined by Johnson's optimizing scheme, to be discussed below. In the controlled experiment, the value of ϵ so determined is used in both the synoptic and radar approaches, so that the two sets of calculations are consistent.

The parameters $\nu_c(\lambda)$ and $\eta(\lambda)$ are not given separate explicit values. Rather, they are considered together in the following way. From (31) and (34), the total rain produced by convective updrafts of cells with entrainment rates of λ to $\lambda + d\lambda$ is

$$[R_c(\lambda) + \phi(\lambda)C_A(\lambda)]d\lambda = \nu'(\lambda)C_u(\lambda)d\lambda, \quad (65)$$

where

$$\nu'(\lambda) = \nu_c(\lambda) + \phi(\lambda)\eta(\lambda), \quad (66)$$

and $\phi(\lambda)$ is the fraction of the condensate $C_A(\lambda)d\lambda$ which is converted to mesoscale rain after it is incorporated into the anvil region. The first term in (65) is the rain that falls directly from cells, while the second term is the amount of water that is condensed in the cells but eventually falls as rain in the anvil region outside the cells. The term $\nu'(\lambda)$ is the efficiency with which $C_u(\lambda)d\lambda$ is converted to precipitation of one kind or the other. Under the assumption of case (b) [Eq. (53)], all of the mesoscale rain R_m is derived from condensate originating in convective cells. Hence, integration of (65) over all λ gives

$$R_T = \nu' C_{UT}, \quad (67)$$

where ν' is assumed to be invariant with λ, C_{UT} is the total convective condensate, given by

$$C_{UT} = \int_0^\infty C_u(\lambda)d\lambda, \quad (68)$$

R_T is the total precipitation, given by

$$R_T = R_{CT} + R_m, \quad (69)$$

and R_{CT} is the total convective rain, given by

$$R_{CT} = \int_0^\infty R_c(\lambda)d\lambda. \quad (70)$$

In the synoptic approach, a value of ϵ is assumed, and R_T and C_{UT} are calculated from the diagnosed cloud properties. The value of ϵ is adjusted until the computed R_T agrees most closely with the observed total precipitation. A value of ν' is then implied by (67). This is Johnson's (1976) optimization scheme for determining ϵ and ν'.

To use ϵ and ν' obtained in this way in the radar approach, instead of the more explicit water budget parameters ν_c, α and η, Eq. (65) is rewritten using (31) and (34) as

$$R_c(\lambda)\left(1 + \frac{\phi\eta}{\nu_c}\right)d\lambda = \nu'(\lambda)C_u(\lambda)d\lambda. \quad (71)$$

The term $\phi\eta/\nu_c$ is the ratio of the portion of the mesoscale rain R_m derived from condensate produced in cells with entrainment rates λ to $\lambda + d\lambda$ to the convective rain $R_c(\lambda)d\lambda$ derived from the same cell. For simplicity, we assume that $\phi\eta/\nu_c$ is a constant. Integrating (71) and substituting from (67) then yields

$$\int_0^\infty R_c(\lambda)\left(1 + \frac{\phi\eta}{\nu_c}\right)d\lambda = \left(1 + \frac{\phi\eta}{\nu_c}\right)R_{CT} = R_T. \quad (72)$$

From (72) and (69), it follows that

$$\frac{\phi\eta}{\nu_c} = \frac{R_m}{R_{CT}}. \quad (73)$$

Substituting (3), (29), (37) and (73) into (71) and rearranging terms leads to

$$(\nu')^{-1}R_c(\lambda)\left(1 + \frac{R_m}{R_{CT}}\right)d\lambda = I_1(\lambda)\mathcal{M}_B(\lambda)d\lambda, \quad (74)$$

which is an alternate form of (36).

In the radar approach calculations for the controlled experiment, we use (74) instead of (36) to calculate $\mathcal{M}_B(\lambda)$ from the radar observed quantities $R_c(\lambda)d\lambda$ and R_m since ν' is known from the synoptic approach and ν_c is not.

In summary, our treatment of assumption (vii) in the controlled experiment determines that the water budget parameters of the diagnostic cloud model described in previous sections are consistent with the parameters assumed in Johnson (1976). In future studies (e.g., Leary and Houze, 1980), we will make alternate cloud water budget assumptions that simulate more realistically tropical cloud ensembles, which include mesoscale anvil cloud circulations as well as convective-scale updrafts and downdrafts. In the controlled experiment described below, we seek only to show that for a particular set of model parameters similar results can be obtained from either synoptic or radar input data.

d. Input data for the controlled experiment

In solving (74) for $\mathcal{M}_B(\lambda)$ in the radar approach we obtain $R_c(\lambda)d\lambda$ and R_m from Cheng and Houze's (1979) precipitation spectrum from Phase III of GATE (their Fig. 2d). Although their spectrum was obtained for only a portion of the GATE observational array and for a subset of the time period of Phase III, it is assumed here that the spectrum was representative of the whole area over the entire phase. Thus, the spectrum is applied to the total GATE B-scale area rainfall, and the factors A and τ

are taken to be the area of the B-scale array and the total time period of Phase III.

Cheng and Houze's precipitation spectrum shows large amounts of rain associated with echoes that had maximum tops above 14 km. However, as they note, the maximum height of a convective echo region typically was attained only temporarily and by a small portion of the total area covered by the convective region. Most of the mass transport producing such convective echoes was probably confined below 14 km. Therefore, we assign all the rain associated with echo tops above 14 km in their spectrum to convective cells with tops of 14 km.

Under the Johnson (1976) assumptions, which we use in the controlled experiment, (60) reduces to (61). In solving for $\mathcal{M}_B(\lambda)$ in the synoptic approach, we use the convective heating function $(-\partial\widetilde{\omega'h'}/\partial p)$ determined by Thompson *et al.* (1979). Thus, the radar and synoptic approach calculations are based on independent sets of data for the same population of clouds.

e. Removal of non-precipitating clouds from the synoptic approach

The $\mathcal{M}_B(\lambda)$ obtained by solving (61) includes the effects of both precipitating and non-precipitating clouds. To compare this $\mathcal{M}_B(\lambda)$ with that obtained by solving (74), which is based on observed precipitation, we remove the effects of non-precipitating clouds from $\mathcal{M}_B(\lambda)$ by subtracting the contributions from clouds with tops below the 600 mb level under the assumption that only the deeper clouds precipitate significantly. This assumption agrees with the results of Cheng and Houze (1979) who found that very little rain came from cells with maximum heights below the 600 mb level during GATE.

f. Comparing the results of the radar and synoptic approaches in the controlled experiment

The only difference between the radar and synoptic approaches in the controlled experiment is in the determination of $\mathcal{M}_B(\lambda)$, which is computed from (61) in the synoptic approach and from (74) in the radar approach.

After obtaining $\mathcal{M}_B(\lambda)$ by *either* approach, the downdraft mass transport spectral function $\mathcal{M}_0(\lambda)$ is determined by (41) using the value of ϵ arrived at by Johnson's optimization scheme, and the bulk updraft and downdraft mass fluxes $M_u(z)$ and $M_d(z)$ are determined from (2) and (16) using the profiles f_u and f_d prescribed by assumption (iii). The moist-static energies in convective updrafts and downdrafts, $h_u(\lambda,z)$ and $h_d(\lambda,z)$, are computed exactly the same way, from (11) and (21), respectively, in both approaches. Thus, differences in $\mathcal{M}_0(\lambda)$, $M_u(\lambda)$, $M_d(\lambda)$, and $(-\widetilde{\omega'h'})$ computed by the two approaches in the controlled experiment arise only inasmuch as there are differences in $\mathcal{M}_B(\lambda)$. Consequently, the most basic comparison to be made is between the values of $\mathcal{M}_B(\lambda)$ computed in each approach.

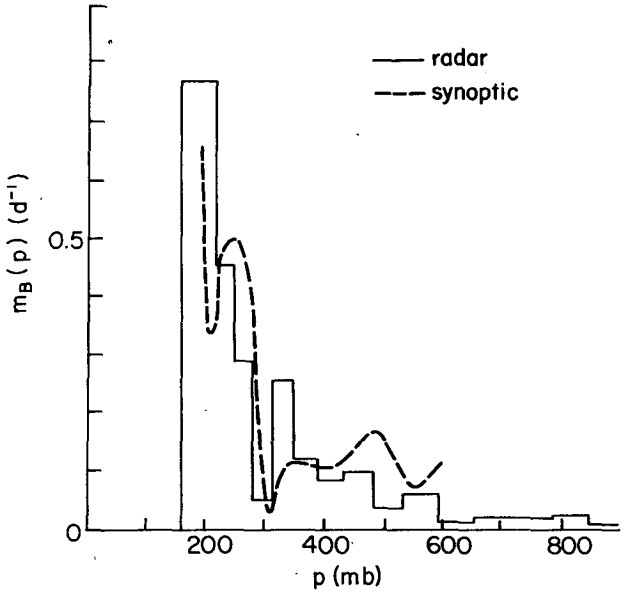

FIG. 5. Cell-base mass transport spectrum diagnosed by the radar and synoptic approaches.

6. Results of the controlled experiment

a. Mass transport spectrum

The values of $\mathcal{M}_B(\lambda)$ computed by the radar and synoptic approaches in the controlled experiment are compared in Fig. 5 by plotting the function $m_B(p)$, defined, following Johnson (1976), as $A^{-1}\tau^{-1} \times \mathcal{M}_B(\lambda)d\lambda_T/dp$, where λ_T is the entrainment rate for cells with tops at level p. The area under the curve $m_B(p)$ is proportional to the total upward mass flux at cloud base $M_u(z = z_B)$. The areas under the radar and synoptic curves in Fig. 5 are within 15% of each other, with the area under the radar curve being slightly larger. The shapes of the curves are also quite similar, showing increasing amounts of mass flux with increasing cell size. Since the maximum cell tops were 14 km (~150 mb) in the radar approach but could be diagnosed to be no greater than 12 km (~175 mb) in the synoptic approach, and since cells with tops below the 600 mb level have been deleted from the synoptic calculations, the domain for the radar curve is greater than for the synoptic curve. However, from the radar curve, which is directly derived from the rainfall spectrum, it can be seen that cells with tops below 600 mb contributed only a negligible portion of the total cloud-base mass flux.

The similarity of the curves in Fig. 5 is dramatic evidence that the radar and synoptic approaches, based on independent data sets, give basically simi-

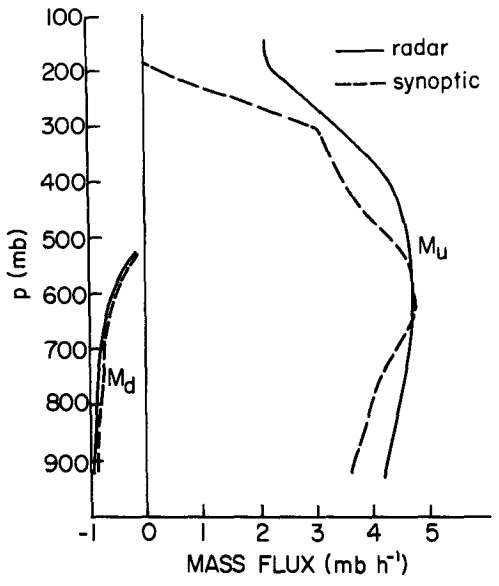

FIG. 6. Bulk mass fluxes by convective updrafts (M_u) and downdrafts (M_d) diagnosed by the radar and synoptic approaches.

lar results. Confidence in both techniques is thus increased. Confidence in the two data sets themselves, the heat budgets derived from the synoptic data set by Thompson *et al.* (1979), and in the precipitation spectrum derived from the radar data set by Cheng and Houze (1979) are also greatly increased.

b. Bulk mass and heat fluxes

The bulk mass and heat fluxes derived by the two approaches are compared in Figs. 6 and 7. The shapes and general magnitudes of the curves are in good agreement at most levels. The radar approach, because of its ability to diagnose the presence of overshooting cells, shows significant mass transport above the 250 mb level, where the synoptically diagnosed mass transports decrease sharply to zero near 200 mb. The overshooting cells produce slight negative heat fluxes above 200 mb.

c. Heat budget

Following Johnson (1976), the total convective heating $-\partial(\widetilde{\omega'h'})/\partial p$, given by (61), may be written as

$$-\frac{\partial\widetilde{\omega'h'}}{\partial p} = Q_1 - Q_2 - Q_R, \tag{75}$$

where Q_1 is the apparent heat source derived from synoptic data, Q_2 the apparent moisture sink (in heating units) similarly derived and Q_R the radiative heating. The sensible heat budget is given by

$$Q_1 - Q_R = \frac{g}{A\tau}\left\{\delta^*(p)[s_u(\lambda_T,p) - \tilde{s}_e] - (M_u + M_d)\frac{\partial\tilde{s}_e}{\partial p} - L\bar{e}_u\right\}, \tag{76}$$

and the moisture budget by

$$-\frac{Q_2}{L} = \frac{g}{A\tau}\left\{\delta^*(p)[q_u(\lambda_T,p) - \tilde{q}_e] - (M_u + M_d)\frac{\partial\tilde{q}_e}{\partial p} + \bar{e}_u\right\}, \tag{77}$$

where s is the dry static energy defined as $c_pT + gz$ and $\bar{e}_u$ is the evaporation of water detrained from convective updrafts.

Three of the terms in the moisture budget equation (76) are plotted in Fig. 8. The agreement between the two approaches is quite good. As in previous diagnostic studies, the dominant term is $-M_u \times \partial\tilde{q}_e/\partial p$, the effect of compensating subsidence drying the large-scale environment [see Johnson (1976) for more discussion]. Since we have removed any contribution from clouds with tops below the 600 mb level, the synoptic approach curve for the term involving detrainment at cloud top, $g\delta^*(q_u - q_e)/A\tau$, is zero below the 600 mb level. The radar approach curve for this term is a histogram since it is derived from a discrete precipitation spectrum.

The term $\bar{e}_u$ in (77), obtained by subtracting the three dashed (synoptic) curves in Fig. 8 from the value of Q_2 obtained in the budget study of Thompson *et al.* (1979), is plotted in Fig. 9. This curve is similar to the ones found by Johnson (1976). Above

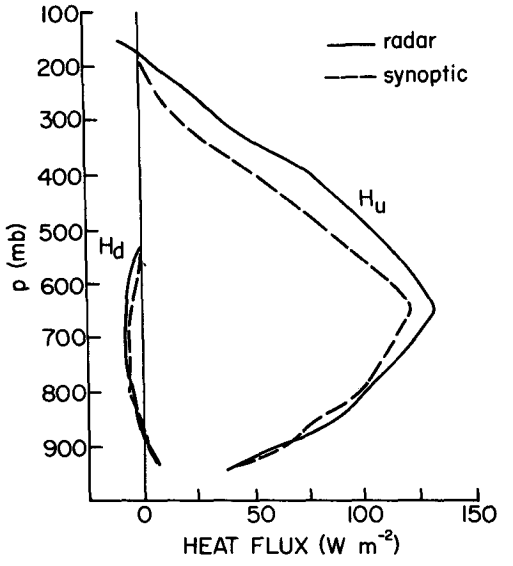

FIG. 7. Bulk heat fluxes by convective updrafts (H_u) and downdrafts (H_d) diagnosed by the radar and synoptic approaches.

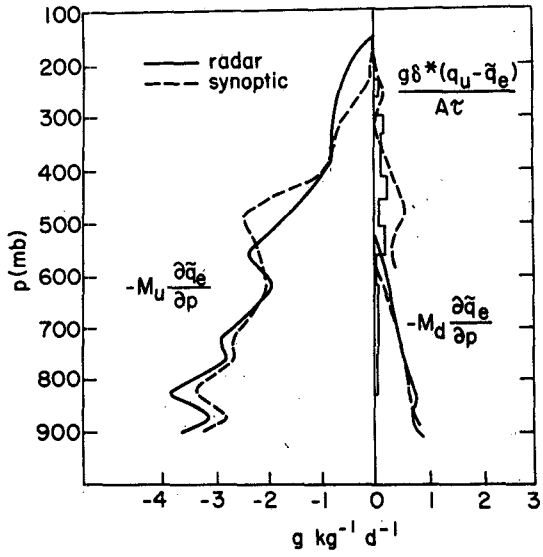

FIG. 8. Contributions to the large-scale moisture budget of vertical motion compensating for convective updrafts ($-M_u\partial\tilde{q}_e/\partial p$) and downdrafts ($-M_d\partial\tilde{q}_e/\partial p$) and of detrainment of water vapor from the tops of cells [$g\delta^*(q_u - \tilde{q}_e)/A\tau$] computed by the radar and synoptic approaches.

400 mb the term is small, actually slightly negative, indicating no evaporation of condensate detrained from cells with tops at these levels. Yet, paradoxically, these are precisely the levels of strong detrainment from the most intense convective cells.

To try to resolve this question, we formulated equations of the form of (8) to calculate the cloud liquid water mixing ratio q_c and the precipitation water mixing ratio q_p as functions of height (or p) in cells of a given λ, using a Kessler parameterization for the source terms (Appendix B). The total detrainment of liquid water at a given p is then calculated as

$$\delta_L(p) \equiv \left(\frac{g}{A\tau}\right)\delta^*(p)\{q_c[\lambda_T(p),p] + q_p[\lambda_T(p),p]\}. \quad (78)$$

As expected, this quantity is quite large above 400 mb in contrast with the small negative value of $\bar{e}_u$ (Fig. 9). This result suggests that the large amount of water detrained from deep convective cells was not being evaporated in the large-scale environment.

Then what happened to the detrained water? We know from the Phase III precipitation spectrum of Cheng and Houze (1979) that a considerable portion of the rain fell as horizontally uniform mesoscale anvil rain R_m. Recall, however, from the discussion of assumption (vii) in Section 5c that to make the radar approach calculations compatible with Johnson's (1976) assumptions, we assumed that the mesoscale rain R_m was condensed in convective-scale cells but transported into the mesoscale anvil regions via the effect represented by the terms $C_A(\lambda)d\lambda$. We conclude from this that the detrained condensate δ_L computed by (78) contributed to the terms $C_A(\lambda)d\lambda$, and thus was assumed in this

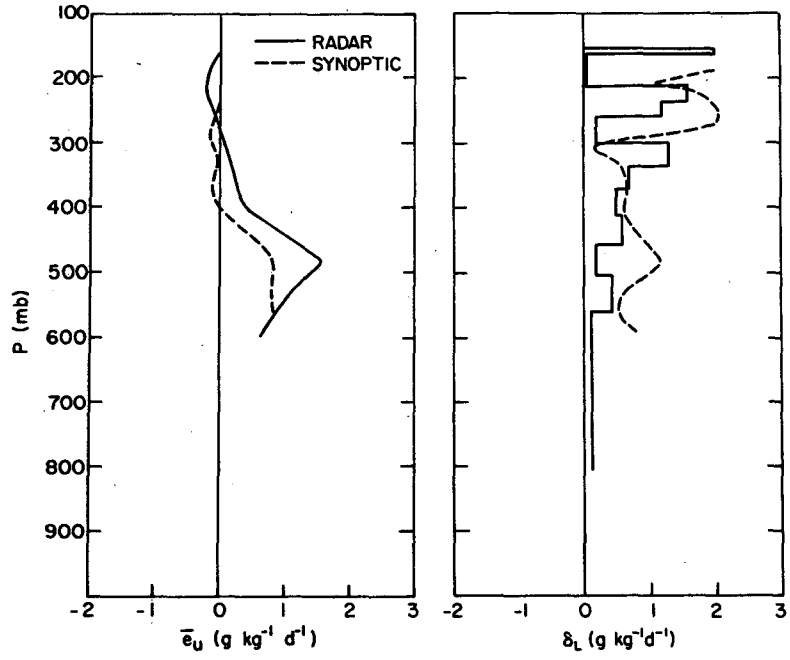

FIG. 9. Evaporation of condensate from detrained cells $\bar{e}_u$, computed by the synoptic approach, compared to the detrainment of liquid water from cells δ_L, computed from Eq. (78).

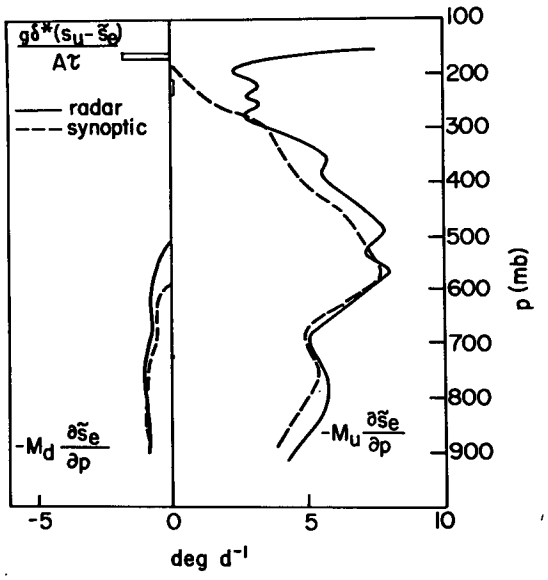

FIG. 10. Contributions to the large-scale heat budget of vertical motion compensating for convective updrafts ($-M_u \partial \bar{s}_e / \partial p$) and downdrafts ($-M_d \partial \bar{s}_e / \partial p$) and of detrainment of dry static energy from the tops of cells [$g\delta^*(s_u - \bar{s}_e)/A\tau$] computed by the radar and synoptic approaches. The detrainment term was so small in the synoptic case that it was not plotted.

formulation of the diagnostic model to enter the anvil clouds and eventually fall as part of the mesoscale rain R_m, rather than be evaporated. Thus, again, we see evidence of the important role of anvil clouds in tropical convective cloud populations.

Terms in the sensible heat budget equation (76) are plotted in Fig. 10. The dominant term, as in the moisture budget, is the compensating subsidence effect, here represented by ($-M_u \partial \bar{s}_e / \partial p$), the dry adiabatic warming of the environment. The radar and synoptic approaches are in good agreement, except above 300 mb, where the deep, overshooting cells, which were detected by radar but not diagnosed in the synoptic approach, had an effect. The effect is largest in the compensating subsidence term.

The magnitude of the compensating subsidence term above 300 mb shown by the radar approach, is somewhat exaggerated in Fig. 10 by the exponential mass transport profiles $f_u(\lambda,z)$, which we have assumed in this controlled experiment. These profiles concentrate the maximum mass transport, and hence, compensating subsidence, at cloud top. Since in the radar case, overshooting cloud tops extend up into layers of high stability (large $\partial s_e / \partial p$) the enhanced compensating subsidence associated with the exponential profiles is strongly felt in the compensating subsidence heating term. Although the same exponential profiles were used in the synoptic approach, the effect does not appear as strongly because the deep, overshooting cells were not detected. When more moderate profiles are assumed, placing the maximum mass transport at some distance below cell top, the magnitude of the compensating subsidence heating at high levels in the radar approach is substantially reduced (Cheng and Houze, 1980).

The effect of the overshooting cells is also seen in the detrainment term [$g\delta^*(s_u - \bar{s}_e)/A\tau$] in Fig. 10. This term is so close to zero in the synoptic approach calculations that it is not plotted, whereas in the radar approach calculations, its effect is noticeable at high levels where overshooting cell tops had significant differences between s_u and $\bar{s}_e$.

7. Conclusions

In this paper, we have diagnosed the mass and heat fluxes by convective clouds in GATE from two independent data sets (radar and synoptic) and obtained similar results. Hence, we conclude that the two sets of data are good, that the spectrum of precipitation derived from the radar data and the large-scale heat and moisture budgets derived from the synoptic data were obtained correctly, and that the diagnostic approaches using the radar and synoptic data as input are basically sound.

The data sets and their analyses have been described in detail elsewhere, the derivation of the precipitation spectrum from radar data by Cheng and Houze (1979) and the determination of heat and moisture budgets from synoptic data by Thompson *et al.* (1979). We will, therefore, focus our concluding remarks on the diagnostic approaches which use the analyzed data as input.

Both diagnostic approaches, the radar and synoptic, begin by postulating a population of model clouds. In the radar approach, the model clouds are constrained to produce the observed spectrum of convective and mesoscale precipitation. In the synoptic approach, the model clouds are constrained to balance the observed synoptic-scale heat and moisture budgets. Under either constraint, the cloud mass flux spectrum can be determined. The population of model clouds which is used in both approaches, however, has various properties which must first be assumed [assumptions (i)–(vii), Section 5b]. From the computed mass flux spectrum and the assumptions (i)–(vii), other properties of the cloud population follow.

For the same synoptic or radar input data, the diagnosed cloud mass flux spectrum varies depending on how the assumptions (i)–(vii) are made. That is, the diagnostic results are model-dependent. In the controlled experiment presented in this paper, the assumptions were treated the same way in both approaches so that differences between the mass flux spectra diagnosed by the two approaches could be attributed to the different data sets on which they were based rather than the differences in model assumptions.

The differences obtained were, in fact, small, each approach giving practically the same cloud mass flux spectrum, except that the radar approach diagnosed the contribution by overshooting convection, which the synoptic approach could not detect, and the synoptic approach diagnosed the mass fluxes by non-precipitating convection, which the radar approach could not detect.

Although the agreement between the approaches is encouraging, for the reasons stated in the first paragraph of this section, it does not mean that the results obtained in the controlled experiment are correct! The cloud population properties diagnosed by the two approaches are certainly consistent, but they are correct only to the extent that the model assumptions (i)–(vii) were made realistically. In the controlled experiment, these assumptions were treated as they have been traditionally, assuming, for example, that detrainment occurs only at cell tops, that cell tops occur at the level of zero buoyancy, that the cells entrain unmodified environmental air, and, most notably, that there are no mesoscale motions associated with precipitating anvil clouds. The latter assumption is probably the most significant insufficiency of current approaches as there is an overwhelming amount of evidence accumulating that mesoscale anvil rain constitutes a substantial portion of the total rain in GATE cloud ensembles and that mesoscale updrafts in the anvils and mesoscale downdrafts below the anvils contribute to the cloud mass and heat fluxes (Zipser, 1977; Houze, 1977; Leary and Houze, 1979a,b; Cheng and Houze, 1979). Even the moisture budget calculations of the controlled experiment itself suggest that precipitation from anvil clouds must have been significant, as hydrometeors detrained from deep convective cells apparently did not evaporate in the large-scale environment (Section 6d). If not, they must have fallen as precipitation from anvil clouds associated with the deep cells.

The equations developed in this paper are general enough to go beyond the traditional assumptions and investigate the differences which arise in the diagnostic results when assumptions (i)–(vii) are varied. Having established the calculations of the controlled experiment of this paper as a baseline, we shall, in future papers, rediagnose the mass and heat transports by the radar approach under different variations of these assumptions. First, we will examine the impacts of varying assumptions (i)–(vi), which deal with the structure of the convective cells themselves (Cheng and Houze, 1980). Second, the changes in diagnosed mass and heat flux profiles that arise when more realistic treatment of the cloud model water budgets [assumption (vii)] is incorporated in the calculations will be examined (Leary and Houze, 1980; Cheng and Houze, in preparation). This more realistic treatment of the water budgets, accomplished by assuming $C_{mu} > 0$ in (50) and $E_{md} > 0$ in (54), will allow the mass and heat transports by mesoscale anvil cloud circulations to be diagnosed along with the convective fluxes.

These diagnostic studies will help clarify the extent to which mesoscale motions associated with precipitating anvil clouds influence large-scale mass and heat budgets. If their influence is significant, as we anticipate, then some re-thinking of convective parameterization schemes that do not take mesoscale motions into account may be necessary.

Acknowledgments. Prof. Richard H. Johnson graciously made his computer programs available to us. Prof. Richard J. Reed provided us with his group's large-scale mass and heat budget calculations and other GATE data analyses. Ilze Schubert typed this manuscript and graphic arts were by Kay Moore. This research was supported by the Global Atmospheric Research Program, Division of Atmospheric Sciences, National Science Foundation and the GATE Project Office, National Oceanic and Atmospheric Administration under Grants ATM74-14830 A01 and ATM78-16859.

APPENDIX A

An Expression for the Convective Heating

The atmospheric heating owing to the vertical convergence of the convective heat flux ($-\widetilde{\omega' h'}$) is obtained by taking the derivative with respect to p of Eq. (59). This derivative is

$$\begin{aligned}\frac{\partial}{\partial p}(-\widetilde{\omega' h'}) = \frac{g}{A\tau}\Bigg[&\delta^*(p)[h_u(\lambda_T,p) - \tilde{h}_e(p)] \\ &+ \int_0^{\lambda_T(p)} \Bigg\{ -\frac{\partial \tilde{h}_e}{\partial p}[\mathcal{M}_u(\lambda,p) + \mathcal{M}_d(\lambda,p)] \\ &+ \delta_u(p)[h_u(\lambda,p) - \tilde{h}_e(p)] \\ &+ \delta_d(p)[h_d(\lambda,p) - \tilde{h}_e(p)] \\ &+ \epsilon_u(p)[\tilde{h}_e(p) - \hat{h}_u(\lambda,p)] \\ &+ \epsilon_d(p)[\tilde{h}_e(p) - \hat{h}_d(\lambda,p)]\Bigg\} d\lambda\Bigg] \\ &+ \frac{\partial}{\partial p}\Bigg\{\Bigg[\frac{g\mu_m}{A\tau} + \widetilde{\sigma_m \omega(p)}\Bigg] \\ &\times [h_m(p) - \tilde{h}_e(p)]\Bigg\}. \quad \text{(A1)}\end{aligned}$$

To obtain (A1), substitution is made from (3), (4), (5), (10), (14), (15) and (20) after they are converted to a p coordinate using

$$dz = -Hd\ln p, \quad \text{(A2)}$$

where H is the scale height of the large-scale environment, and the following definitions are used:

$$\delta^*(p) \equiv \frac{d\lambda_T}{dp}\mathcal{M}_u(\lambda_T,p) = \frac{d\lambda_T}{dp}f_u[\lambda_T,z(p)]\mathcal{M}_B(\lambda_T), \quad \text{(A3)}$$

$$\epsilon_u(p) \equiv -\left[\frac{\partial \mathcal{M}_u(\lambda,p)}{\partial p}\right]_\epsilon, \quad \text{(A4)}$$

$$\epsilon_d(p) \equiv -\left[\frac{\partial \mathcal{M}_d(\lambda,p)}{\partial p}\right]_\epsilon, \quad \text{(A5)}$$

$$\delta_u(p) \equiv \left[\frac{\partial \mathcal{M}_u(\lambda,p)}{\partial p}\right]_\delta, \quad \text{(A6)}$$

$$\delta_d(p) \equiv \left[\frac{\partial \mathcal{M}_d(\lambda,p)}{\partial p}\right]_\delta. \quad \text{(A7)}$$

Using (3), (4), (5), (14), (15), (41), and (A2) we can show that all five of these quantities are proportional to $\mathcal{M}_B(\lambda)$. Specifically,

$$\epsilon_u(p) = \underbrace{+(\lambda H/p)f_u[\lambda,z(p)]}_{a_1(\lambda,p)}\mathcal{M}_B(\lambda), \quad \text{(A8)}$$

$$\epsilon_d(p) = \underbrace{-(\lambda H/p)f_d[\lambda,z(p)]\epsilon(\lambda)}_{a_2(\lambda,p)}\mathcal{M}_B(\lambda), \quad \text{(A9)}$$

$$\delta_u(p) = \underbrace{\left\{\frac{\partial f_u[\lambda,z(p)]}{\partial p} + \frac{\lambda H}{p}f_u[\lambda,z(p)]\right\}}_{a_3(\lambda,p)}\mathcal{M}_B(\lambda), \quad \text{(A10)}$$

$$\delta_d(p) = \underbrace{\left\{\frac{\partial f_d[\lambda,z(p)]}{\partial p} - \frac{\lambda H}{p}f_d[\lambda,z(p)]\right\}\epsilon(\lambda)}_{a_4(\lambda,p)}\mathcal{M}_B(\lambda). \quad \text{(A11)}$$

Substituting (3), (17), (41), (A3) and (A8)–(A11) into (A1), we obtain Eq. (60), in which

$$f_1(p) = \frac{\partial}{\partial p}\left\{\frac{g\mu_m}{A\tau} + \sigma_m\widetilde{\omega(p)}[h_m(p) - \tilde{h}_e(p)]\right\}, \quad \text{(A12)}$$

$$f_2(p) = \frac{g}{A\tau}\frac{d\lambda_T}{dp}f_u[\lambda_T,z(p)][h_u(\lambda_T,p) - \tilde{h}_e(p)], \quad \text{(A13)}$$

$$f_3(p) = -\frac{\partial \tilde{h}_e}{\partial p}\{f_u[\lambda,z(p)] + \epsilon(\lambda)f_d[\lambda,z(p)]\} + a_1(\lambda,p)[\tilde{h}_e(p) - \hat{h}_u(\lambda,p)] + a_2(\lambda,p)[\tilde{h}_e(p) - \hat{h}_d(\lambda,p)] + a_3(\lambda,p)[h_u(\lambda,p) - \tilde{h}_e(p)] + a_4(\lambda,p)[h_d(\lambda,p) - \tilde{h}_e(p)]. \quad \text{(A14)}$$

In (A12), the term involving μ_m can be evaluated if the precipitation quantities R_m and $R_c(\lambda)$ are measured since from (23), (24), (25), (31), (34), (36), (45), (50) and (56), we have

$$\mu_m(p) = \begin{cases} \mu_{mu}[z(p)] = \dfrac{R_m f_{mu}[z(p)]}{I_3\nu_m} - \displaystyle\int_0^\infty \frac{\eta(\lambda)R_c(\lambda)}{\nu_c I_3}, & p \leq p(z_m) \\ \mu_{md}[z(p)] = \dfrac{aR_m f_{md}[z(p)]}{I_4\nu_m}, & p < p(z_m). \end{cases} \quad \text{(A15)}$$

To evaluate the term involving $\widetilde{\sigma_m\omega(p)}$ in (A12), some observation or assumption regarding this quantity must be made.

APPENDIX B

Computation of the Precipitation Water Content in Convective Updrafts

Following Kessler (1969), the hydrometeor content (ignoring the ice phase) can be divided into two categories, cloud liquid water content, defined as

$$m_c(\lambda,z) \equiv \rho q_c(\lambda,z), \quad \text{(B1)}$$

where ρ is the density of air, and the precipitation liquid water content, defined as

$$m_p(\lambda,z) \equiv \rho q_p(\lambda,z). \quad \text{(B2)}$$

We calculate m_c and m_p, and then use an appropriate density to convert them to q_c and q_p, respectively, for substitution into (78).

Using Kessler's (1969) parameterization scheme for cloud microphysical processes, equations for m_c and m_p in a one-dimensional convective updraft are

$$\frac{\partial m_c(\lambda,z)}{\partial z} = G - \left[\frac{AC + CC}{w_u(\lambda,z)}\right] - \lambda m_c(\lambda,z) + m_c(\lambda,z)\frac{\partial \ln\rho}{\partial z} \quad \text{(B3)}$$

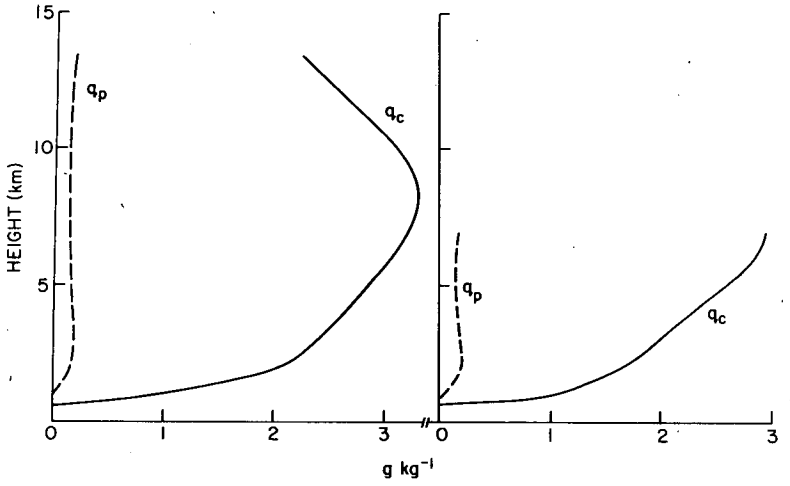

FIG. B1. Mixing ratios of cloud (q_c) and precipitation water (q_p) computed by the scheme described in Appendix B for cells with tops of 6.9 and 13.3 km.

and

$$\frac{\partial m_p(\lambda,z)}{\partial z} = -F + \left[\frac{AC + CC}{w_u(\lambda,z)}\right] - \lambda m_p(\lambda,z) - m_p(\lambda,z)\frac{\partial \ln\rho}{\partial z}, \quad \text{(B4)}$$

where $w_u(\lambda,z)$ is the updraft vertical velocity, G the condensation of water vapor, AC the auto-conversion of cloud liquid water into precipitation, CC the collection of cloud sized droplets by precipitation particles, F the fallout of precipitation, $-\lambda m_c$ and $-\lambda m_p$ the entrainment of cloud and precipitation water, respectively, and $\partial \ln\rho/\partial z$ the air compressibility factor.

It is assumed that the updraft is saturated and that vertical advection of water vapor just balances condensation. Under these conditions,

$$G = -\rho\frac{\partial q_s}{\partial z}, \quad \text{(B5)}$$

where q_s is the saturation mixing ratio. Following Kessler (1969), we let

$$AC = \begin{cases} k_1(m_c - m_0), & m_c > m_0 \\ 0, & \text{otherwise} \end{cases} \quad \text{(B6)}$$

and

$$CC = 0.29N_0^{1/8}m_c m_p^{7/8}\exp(k_2 z/2), \quad \text{(B7)}$$

where $k_1 = 10^{-3}$ s^{-1}, $m_0 = 0.5$ g m^{-3}, $N_0 = 10^7$ m^{-4} and $k_2 = 10^{-4}$ m^{-1}. The fallout of precipitation is calculated by the scheme of Howell and Lopez (described by Cotton, 1972) which assumes that the part of the precipitation water composed of particles with terminal velocities V in excess of the vertical air velocity w is lost to an updraft parcel at the end of each vertical step Δz of the particle's rise. Thus, in finite-difference form,

$$F = (\Delta z)^{-1}\int_{D_w}^{\infty} M_D N(D)dD = (\Delta z)^{-1}\int_{D_w}^{\infty}\frac{\pi\rho_L D^3}{6}N_0 e^{-\Lambda D}dD, \quad \text{(B8)}$$

where M_D is the mass of a drop of diameter D, $N(D)dD$ the number of drops of diameter D to $D + dD$ per unit volume of air and D_w the diameter of a drop whose terminal velocity $V = w$. The relationship between V and D is assumed to be that of Gunn and Kinzer (1949). In the right-hand term in (B8), ρ_L is the density of liquid water and the Marshall-Palmer (1948) distribution $N_0\exp(-\Lambda D)$ has been assumed for $N(D)$. Following Kessler (1969), the parameter Λ is given by $7.49N_0^{1/4}m_p^{-1/4}$.

In a complete one-dimensional updraft model, the vertical velocity $w_u(\lambda,z)$ would be calculated in a simultaneous solution of the vertical equation of motion, the First Law of Thermodynamics and the water continuity equations (B3) and (B4) (e.g., Simpson and Wiggert, 1969, 1971). Since we are just interested here in a reasonable estimate of q_c and q_p for Eq. (78), we avoid the more elaborate model calculation by prescribing a vertical velocity $w_u(\lambda,z)$ for substitution into (B3) and (B4). The vertical velocity profile is assumed to be consistent with the mass flux profile $f_u(\lambda,z)$ such that

$$w(\lambda,z) = w(\lambda,z_B)\frac{\rho(z_B)}{\rho(z)}f_u(\lambda,z). \quad \text{(B9)}$$

The cloud-base vertical velocity $w(\lambda,z_B)$ is parameterized in terms of cell top height z_T according to the relationship

$$w(\lambda,z_B) = \frac{w_{MAX}[\lambda(z_T)]\rho(z_T)}{\rho(z_B)f_u[\lambda(z_T),z_T]}, \quad \text{(B10)}$$

which is obtained by substituting z_T for z in (B9) and solving for $w(\lambda,z_B)$. The value of $w_{MAX}[\lambda(z_T)]$ in (B10) is obtained from Table 1 of Austin and Houze (1973). Eqs. (B3) and (B4) are solved for $m_c(\lambda,z)$ and $m_p(\lambda,z)$. Examples of solutions for clouds of z_T = 6.9 and 13.3 km are shown in Fig. B1.

REFERENCES

Arakawa, A., and W. Schubert, 1974: Interaction of a cumulus cloud ensemble with the large-scale environment. Part I. *J. Atmos. Sci.*, **31**, 674–701.

Austin, P. M., and R. A. Houze, Jr., 1973: A technique for computing vertical transports by precipitating cumuli. *J. Atmos. Sci.*, **30**, 400–411.

Betts, A. K., and M. F. Silva Dias, 1979: Unsaturated downdraft thermodynamics in cumulonimbus. *J. Atmos. Sci.*, **36**, 1061–1071.

Brown, J. M., 1979: Mesoscale unsaturated downdrafts driven by rainfall evaporation: A numerical study. *J. Atmos. Sci.*, **36**, 313–338.

Cheng, C.-P., and R. A. Houze, Jr., 1979. The distribution of convective and mesoscale precipitation in GATE radar echo patterns. *Mon. Wea. Rev.*, **107**, 1370–1381.

——, and ——, 1980: Sensitivity of diagnosed convective fluxes to model assumptions. *J. Atmos. Sci.*, **37**, 774–783.

Cotton, W. R., 1972: Numerical simulation of precipitation development in supercooled cumuli—Part II. *Mon. Wea. Rev.*, **100**, 764–784.

Gunn, R., and G. D. Kinzer, 1949: The terminal velocity for water droplets in stagnant air. *J. Meteor.*, **6**, 243–248.

Houze, R. A., Jr., 1973: A climatological study of vertical transports by cumulus convection. *J. Atmos. Sci.*, **30**, 1112–1123.

——, 1977: Structure and dynamics of a tropical squall-line system. *Mon. Wea. Rev.*, **105**, 1540–1567.

——, and C. A. Leary, 1976: Comparison of convective mass and heat transports in tropical easterly waves computed by two methods. *J. Atmos. Sci.*, **33**, 424–429.

Johnson, R. H., 1976: The role of convective-scale precipitation downdrafts in cumulus and synoptic-scale interactions. *J. Atmos. Sci.*, **33**, 1890–1910.

——, 1977: The effects of cloud detrainment on the diagnosed properties of cumulus populations. *J. Atmos. Sci.*, **34**, 359–366.

——, 1980: Diagnosis of convective-scale and mesoscale motions during Phase III of GATE. *J. Atmos. Sci.*, **37**, 733–753.

Kessler, E., 1969: On the distribution and continuity of water substance in atmospheric circulations. *Meteor. Monogr.*, No. 32, 84 pp.

Leary, C. A., and R. A. Houze, Jr., 1979a: Melting and evaporation of hydrometeors in precipitation from the anvil clouds of deep tropical convection. *J. Atmos. Sci.*, **36**, 669–679.

——, and ——, 1979b: The structure and evolution of convection in a tropical cloud cluster. *J. Atmos. Sci.*, **36**, 437–457.

——, and ——, 1980: The contribution of mesoscale motions to the mass and heat fluxes of an intense tropical convective system. *J. Atmos. Sci.*, **37**, 784–796.

López, R. E., 1973: Cumulus convection and larger scale circulations: II. Cumulus and mesoscale interactions. *Mon. Wea. Rev.*, **101**, 856–870.

Marshall, J. S., and W. McK. Palmer, 1948: The distribution of raindrops with size. *J. Meteor.*, **5**, 165–166.

Nitta, T., 1975: Observational determination of cloud mass flux distributions. *J. Atmos. Sci.*, **32**, 73–91.

——, 1977: Response of cumulus updraft and downdraft to GATE A/B-scale motion systems. *J. Atmos. Sci.*, **34**, 1163–1186.

Ogura, Y., and H. R. Cho, 1973: Diagnostic determination of cumulus cloud populations from observed large-scale variables. *J. Atmos. Sci.*, **30**, 1276–1286.

Simpson, J., and V. Wiggert, 1969: Models of precipitating cumulus towers. *Mon. Wea. Rev.*, **97**, 471–489.

——, and V. Wiggert, 1971: 1968 Florida cumulus seeding experiment: Numerical model and results. *Mon. Wea. Rev.*, **99**, 87–118.

Thompson, R. M., S. W. Payne, E. E. Recker and R. J. Reed, 1979: Structure and properties of synoptic-scale wave disturbances in the intertropical convergence zone of the eastern Atlantic. *J. Atmos. Sci.*, **36**, 53–72.

Warner, C., J. Simpson, G. van Helvoirt, D. W. Martin, D. Suchman and G. L. Austin, 1980: Deep convection on day 261 of GATE. *Mon. Wea. Rev.*, **108**, 169–194.

Yanai, M., S. Esbensen and J. H. Chu, 1973: Determination of bulk properties of tropical cloud clusters from large-scale heat and moisture budgets. *J. Atmos. Sci.*, **30**, 611–627.

Zipser, E. J., 1969: The role of organized unsaturated convective downdrafts in the structure and rapid decay of an equatorial disturbance. *J. Appl. Meteor.*, **8**, 799–814.

——, 1977: Mesoscale and convective-scale downdrafts as distinct components of squall-line circulation. *Mon. Wea. Rev.*, **105**, 1568–1589.

——, and C. Gautier, 1978: Mesoscale events within a GATE tropical depression. *Mon. Wea. Rev.*, **106**, 789–805.